Science Advances
AAAS

advances.sciencemag.org/cgi/content/full/6/15/eaax2746/DC1

Supplementary Materials for

Targeting the scaffolding role of LSD1 (KDM1A) poises acute myeloid leukemia cells for retinoic acid–induced differentiation

Roberto Ravasio, Elena Ceccacci, Luciano Nicosia, Amir Hosseini, Pier Luigi Rossi, Iros Barozzi, Lorenzo Fornasari, Roberto Dal Zuffo, Sergio Valente, Rossella Fioravanti, Ciro Mercurio, Mario Varasi, Andrea Mattevi, Antonello Mai, Giulio Pavesi, Tiziana Bonaldi, Saverio Minucci*

*Corresponding author. Email: saverio.minucci@ieo.it

Published 8 April 2020, *Sci. Adv.* **6**, eaax2746 (2020)
DOI: 10.1126/sciadv.aax2746

The PDF file includes:

Other Supplementary Material for this manuscript includes the following:

(available at advances.sciencemag.org/cgi/content/full/6/15/eaax2746/DC1)

Supplementary Materials

Materials and Methods

Protein extraction and western blot

Cells were counted and directly lysed in 2X SDS Laemmli buffer (50mM Tris HCl, 10% glycerol, 2% SDS and water) plus protease inhibitors. 80 µg of proteins were mixed with ß-mercaptoethanol and bromophenol blue and denaturated for 8 min at 95°C. Cell lysates were loaded onto polyacrylamide gel and run in SDS Running Buffer. Transfer to nitrocellulose membranes was performed at 100V for 1 hour at 4°C or overnight at 30V in Transfer Buffer containing 20% methanol. Membranes were blocked in 10% milk/ TBS-Tween for 1 hour at room temperature or overnight at 4°C and then probed with primary antibodies diluted in TBS-Tween + 5% milk at 4°C for 2h or overnight. After three washes with TBS-Tween (5 minutes each), membranes were incubated with the appropriate secondary antibody in TBS-Tween+ 5 % milk for 30 min at room temperature. After 3 more washes, signals were revealed using the ECL (Enhanced Chemiluminescence) method.

Chromatin immunoprecipitation (ChIP) and ChIP-seq analyses

Cells were cross-linked in culture medium with 1% formaldehyde and the reaction was stopped after 10 min at RT by adding 0.125 M glycine for 5 min at 4°C. The cells were washed twice with PBS and collected by centrifugation. Pellets were stored at -80° in SDS buffer (50 mM Tris•HCl pH 8.1, 0.33% SDS, 150mM NaCl, 5 mM EDTA, and protease inhibitor cocktail) or directly processed. Fixed cells were resuspended in IP buffer (100mM tris pH 8.6 0.3% SDS 1.7% TRITON x-100 and 5mM EDTA). Chromatin was then fragmented to obtain ~300 bp in average size length by using a Branson Sonifier 250. Chromatin pre-clearing was obtained with protein A-sepharose beads (Amersham). Then, the supernatant was immunoprecipitated overnight in the presence of 30-50 µl of protein G magnetic beads. For histone modification studies, a volume corresponding to $3x10^6$ cells per each IP and 4ug/ml primary antibody were used; for LSD1, GFI1 and PML Chip-Seq, we used $40x10^6$ cells and 10ug/ml of primary antibody. 2.5% of input was stored prior to the de-crosslinking procedure. De-crosslinking was performed for all the IP samples and corresponding inputs, overnight in 0.1%SDS and 0.1% $NaHCO_3$. The day after, the enriched DNA was treated with proteinase K at 56°C for 40 min and purified with a DNA purification kit (Qiagen).

ChIP- Seq analysis

Short reads obtained from Illumina HiSeq 2000 were quality-filtered according to the Illumina pipeline. Analysis of the datasets was automated using the Fish the ChIPs pipeline (*40*) and includes alignment to the hg18 reference genome using Bowtie v1.0.1 (*41*) and MACS version 1.4.1 (Zhang et al., 2008) as peak caller to identify regions of ChIP-seq enrichment over background. Only reads with a unique match to the genome and with two or fewer mismatches (-m 1 –v 2) were retained. MACS was used with a p-value threshold of 10^{-5} for all the data sets except for the LSD1 ChIP where the thresholds were set by qPCR validation. Each sample was compared to input DNA derived from NB4 cells (DMSO). When calling differentially enriched regions among treated and untreated samples, we filtered the resulting regions, keeping only those found enriched against the input. All the lists were annotated over RefSeq genes according to GIN (*42*) while intergenic regions were considered as those at a distance higher than 22kb from the nearest gene. The bigwig files for UCSC browser visualization of genome profiles were normalized with the deepToos suite (*43*) using RPCG.

RNA sequencing and data analysis

mRNA-seq libraries were prepared according to the True-seq Low sample protocol (Illumina, San Diego, California USA), starting with 1ug of total RNA per sample. Raw reads were mapped to the human reference genome hg18 using TopHat2 package (*41*) obtaining comparable number of reads among the samples. Differentially expressed genes were determined using Cufflinks and CuffDiff (*44*). Using the normalized RPKM counts for each sample, we first added a pseudo count to the data which was chosen to be the smallest non-zero value. Genes with a fold change greater than absolute Log2(1.5) respect to DMSO, FDR$\leq$ 0.05 and FPKM $\geq$ 0.5 were defined as differentially expressed genes. Pathway analysis of supplementary figures 5D and 8A was performed with QIAGEN's Ingenuity Pathway Analysis (IPA, QIAGEN Redwood City, www.qiagen.com/ingenuity). Gene onthology of fig 2C was performed through DAVID and visualized by a custom script in R.

Subcellular fractionation

For the preparation of cellular sub-fractions, cells were harvested, washed twice with PBS and resuspended in 3 volumes of Hypotonic Buffer (10 mM Tris HCl pH 7.6, 1.5 mM $MgCl_2$, 10 mM KCl, 1X Roche Protease Inhibitors, 0.5 mM PMSF). After 10 minutes on ice, 1/30 of the original volume of Triton 10% was added to the cells resuspended in Hypotonic Buffer. Cells were vortexed for 30 seconds and centrifuged for 1 minute at 11000 rpm. The supernatant (representing the fraction enriched of cytoplasmic protein) was collected and the pellet (corresponding to the fraction enriched of nuclei) was re-suspended in 2 volumes of Nuclear Extraction

Buffer (50 mM Tris HCl pH 7.6, 150 mM NaCl, 0.5% NP-40, 20% Glycerol, 2 mM $MgCl_2$, 1:100 Benzonase). The suspension was rocked 1h at 4°C and, then, centrifuged at 13000 rpm for 30 minutes. The supernatant, representing the nucleosol fraction, was collected and used for the subsequent immuno-precipitation analyses.

Mass-spectrometry data analysis

Acquired Raw MS data were analyzed with the integrated MaxQuant software v.1.6.0.1, using the Andromeda search engine (*45*); (*46*). The February 2018 version (UniProt Release 2018_02) of the Uniprot sequence was used for peptide identification. Enzyme specificity was set to Trypsin/P, meaning that trypsin cleavage occurs also in the presence of proline, after lysine or arginine residues. In MaxQuant, the estimated false discovery rate (FDR) of all peptide identifications was set to a maximum of 1%. A maximum of 3 missed cleavages was permitted, and the minimum peptide length was fixed at 7 amino acids. Carbamidomethylation of cysteine was set as a fixed modification. 'Requantify' and 'Match between runs' were enabled.

MS-based histone PTM profiling

Cells were homogenized in lysis buffer (10% sucrose, 0.5 mM EGTA, 60 mM KCl, 15 mM NaCl, 15 mM HEPES, 0.5 mM PMSF, 5 µg/ml Aprotonin, 5 µg/ml Leupeptin, 1 mM DTT, 5 mM NaButirrate, 5 mM NaF, 30 µg/ml Spermine, 30 µg/ml Spermidine and 0.5% Triton X-100) and nuclei were separated from cytoplasm by centrifugation on sucrose cushions for 30 minutes at 3750 rpm. Then, histones were extracted through 0.4 N hydrochloric acid for 5 hours at 4°C. Extracted histones were lyophilized, resuspended in milliQ water and quantified by Bradford assay. 5 µg of histones were in-solution digested prior to LC-MS/MS analysis through the hybrid chemical labelling "Pro-PIC" method. This approach is based on an initial conversion of free lysines to their propionylated forms under mild aqueous conditions followed by trypsin digestion and labelling of new peptide N-termini with phenyl isocyanate (PIC) (*47*). The digested peptides were desalted and concentrated by reversed-phase chromatography onto micro-column C18 Stage Tips. Peptides were then eluted from the stage tips with Elution Buffer (60% ACN, 0.1% trifluoroacetic acid), lyophilized, re-suspended in 1% trifluoroacetic acid and subjected to LC-MS/MS analysis. The samples were analysed onto a Hybrid Quadrupole-Orbitrap Q Exactive Mass Spectrometer, upon separation with a gradient of 10-40% solvent B over 100 min, followed by a gradient of 40-60% for 10 min and 60-95% over 3 min at a flow rate of 250 nL/min. MaxQuant software v.1.6.0.1 is used for the analysis of MS data, for both protein and peptides identification including as variable modifications mono-, di- and tri-methyl lysine, mono- and di- methyl arginine and lysine acetylation. The Uniprot HUMAN histones 1502 database was used for histone peptide identification. Enzyme specificity was set to ArgC, since the propionylation of lysine residues allows the trypsin cutting only at the C-terminal of arginine residues. A maximum of 3 missed cleavages were permitted, and the minimum peptide length was fixed at 6 amino acids. PIC at the N-terminal of each peptide was set as a fixed modification. Histone modifications were quantified by label-free approach, in particular by calculating the area under the curve (AUC) of each modified histone peptide and, then extrapolating the percentage relative abundance (%RA), which corresponds to the ratio of the AUC of each individual modified peptide over the sum of the AUC of all modified isoforms of the same peptide.

Supplementary Figures

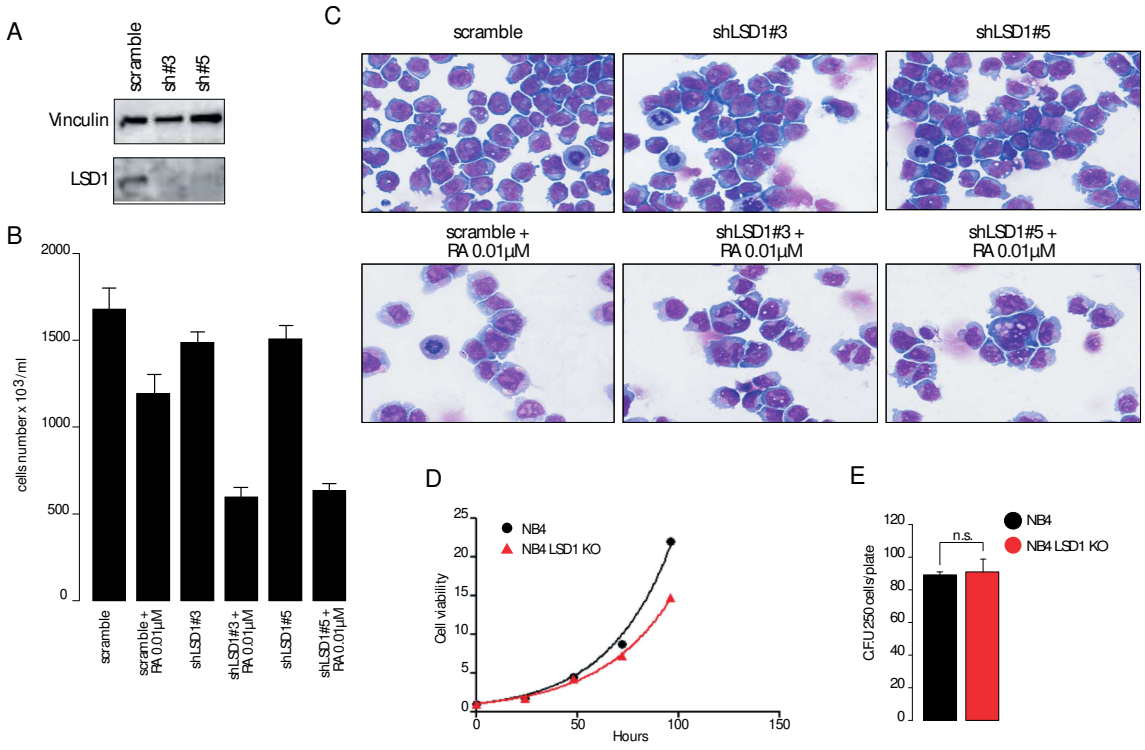

Figure S1. LSD1 knock-down and knock-out recapitulates LSD1 inhibition.
A) Western blot analysis of LSD1 levels in NB4 cells transduced with constructs sh#3 and sh#5 (targeting LSD1). A scrambled sequence was used as experimental control. Vinculin served as loading control. **B)** NB4 cells were transduced with the indicated vectors and treated for 96 hours in liquid culture with RA 0.01µM or DMSO as control. **C)** Morphological analysis (May Grümwald-Giemsa staining) of NB4 cells treated as described for 96 hours in liquid culture **D)** Analysis of cell viability of NB4 and NB4 LSD1 KO cells in liquid culture at 24, 48, 72, 96 hours. Y-axes indicates cell viability (Cell-Titer Glo luminescence) normalized to time 0. **E)** Colony forming ability of NB4 and NB4 LSD1 KO cells plated in methylcellulose medium. Mean and standard deviation of three independent experiments are shown. Two-tailed unpaired Student's t-test, n.s. = not significant.

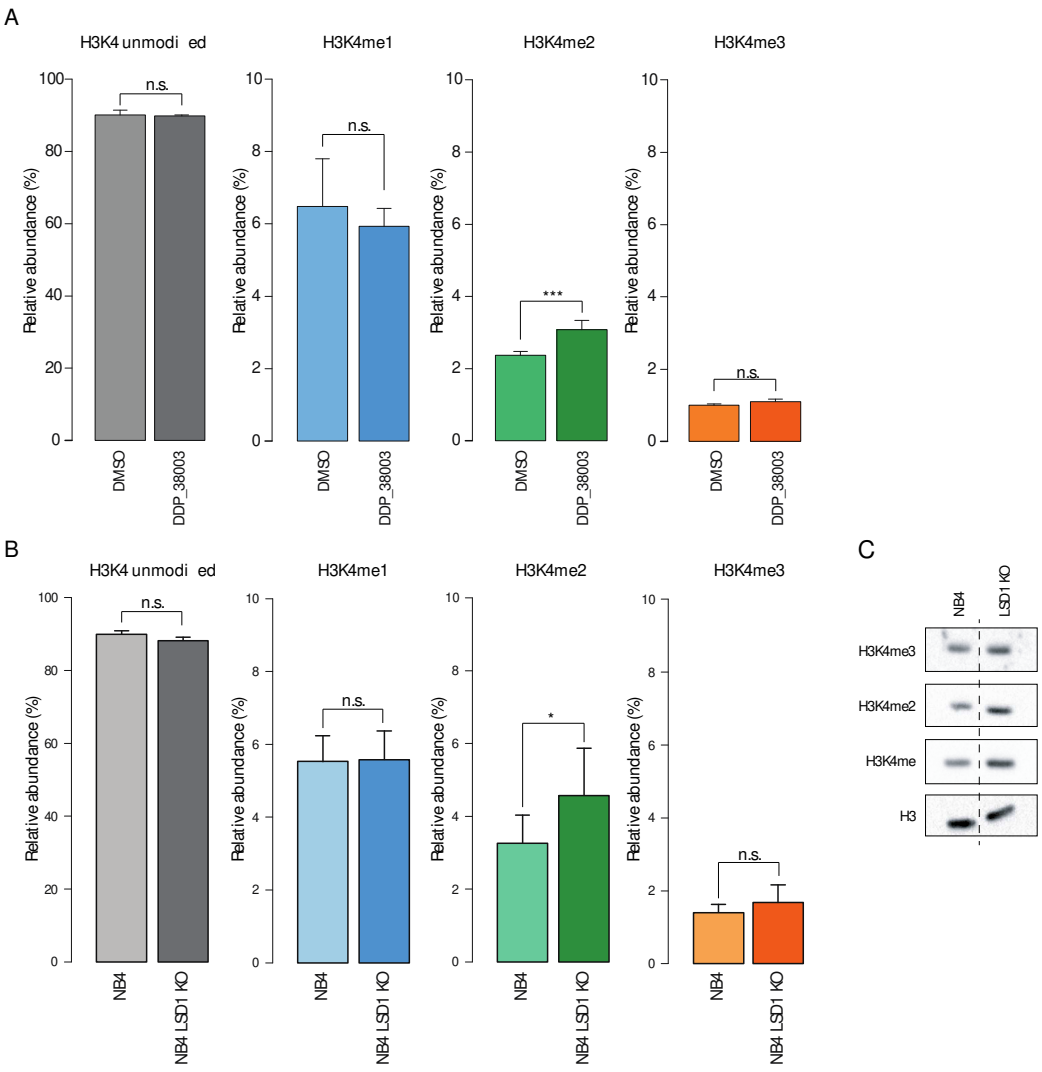

Figure S2. LSD1 inhibition or Knock-Out induce H3K4 methylation accumulation.
A) Mass Spectrometry- based quantification of the differently modified isoforms of H3(3-8) peptide, bearing unmodified, H3K4me1, H3K4me2 and H3K4me3. Histones were purified by strong acid extraction of nuclei from NB4 cells treated with DDP_38003 and DMSO as control (measurements were obtained with 3 biological replicates and 3 technical replicates for each biological replicate). P-values were obtained by two-tailed paired Student's t-test (n.s. = not significant; *** $p < 0.001$). **b)** Mass Spectrometry- based quantification of the differently modified isoforms of H3(3-8) peptide, bearing unmodified, H3K4me1, H3K4me2 and H3K4me3. Histones were fractionated by strong acid extraction of nuclei from wild type and LSD1 KO NB4 cells (n = 3 each). P-values were obtained by two-tailed paired Student's t-test (n.s. = not significant; * $p < 0.05$). **C)** Western blot analysis of H3K4me, H3K4me2 and H3K4me3 in NB4 and NB4 KO cells. H3 served as loading control. Dashed line indicates that lanes have been cropped and paired from the same original membrane.

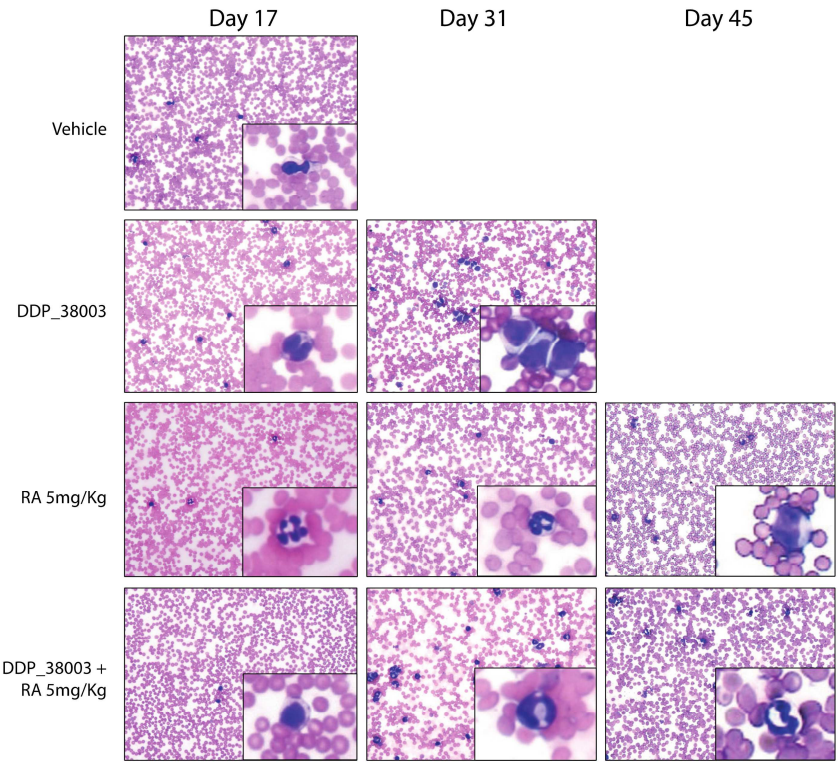

Figure S3. LSD1 inhibition potentiates the therapeutic effect of RA.
May Grümwald-Giemsa staining of blood smears of mice treated as indicated (see Figure 1i).

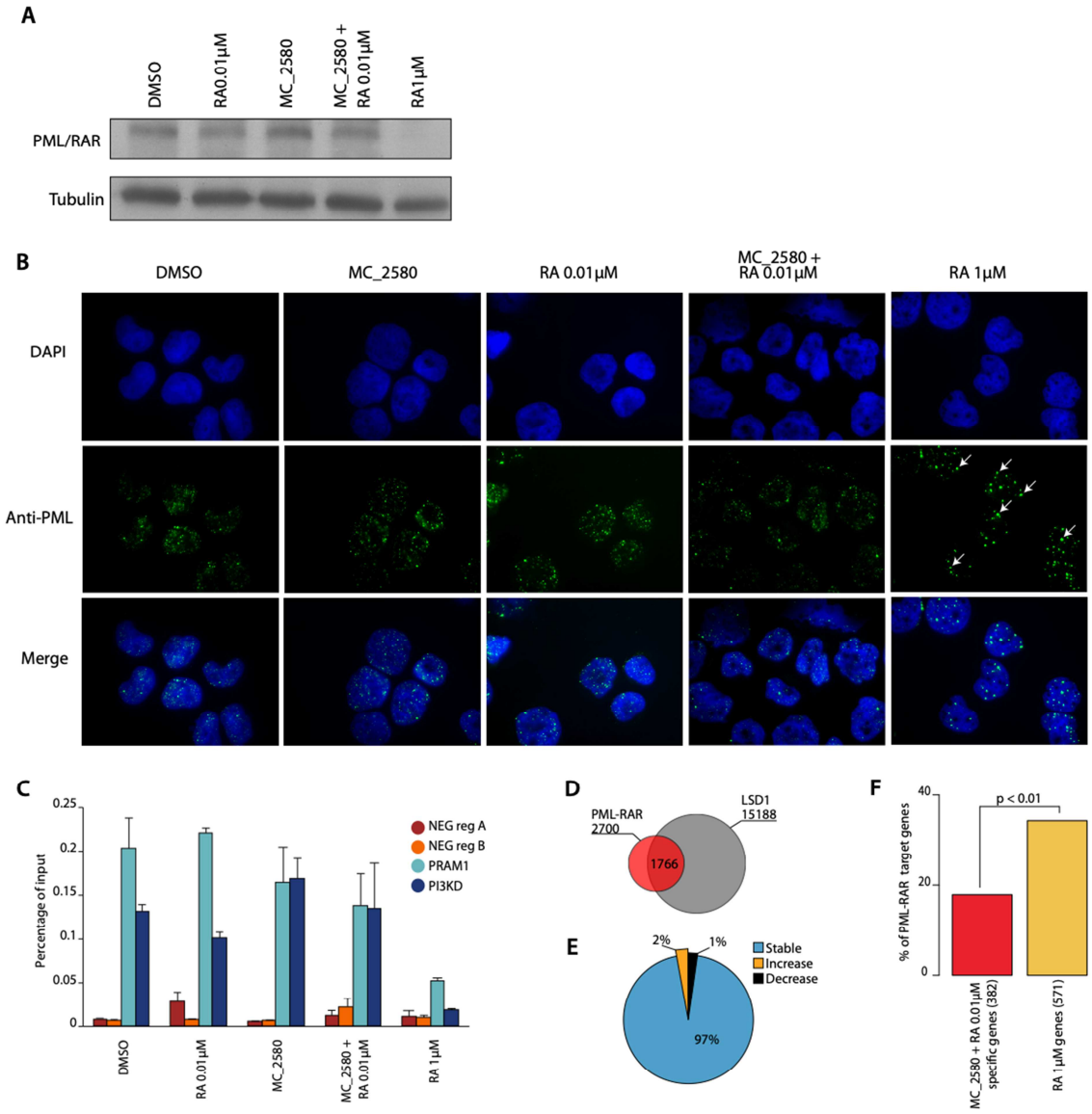

Figure S4. LSD1 inhibition allows APL cells differentiation bypassing PML-RAR function.
A) Western blot analysis of PML-RAR levels in NB4 cells treated as indicated for 24 hours. Tubulin served as loading control. **B)** Representative images showing immunostaining of PML in NB4 cells treated as indicated. Nuclei are identified by DAPI staining. White arrows indicate examples of PML nuclear bodies. **C)** PML-RAR recruitment at target genes assessed by ChIP-qPCR . The results represent percentage of input chromatin and error bars indicate in NB4 cells s.d. from triplicate experiments. **D)** Venn diagram of ChIP-Seq peaks of LSD1 and PML-RAR in NB4 cells. **E)** Pie chart representing the percentage of stable, increasing and decreasing LSD1 ChIP-Seq peaks in PR9 cells before and after PML-RAR induction. **F)** Barplot representing the percentage of PML-RAR targets in genes specifically activated by MC_2580 and RA 0.01µM or activated by RA 1µM.

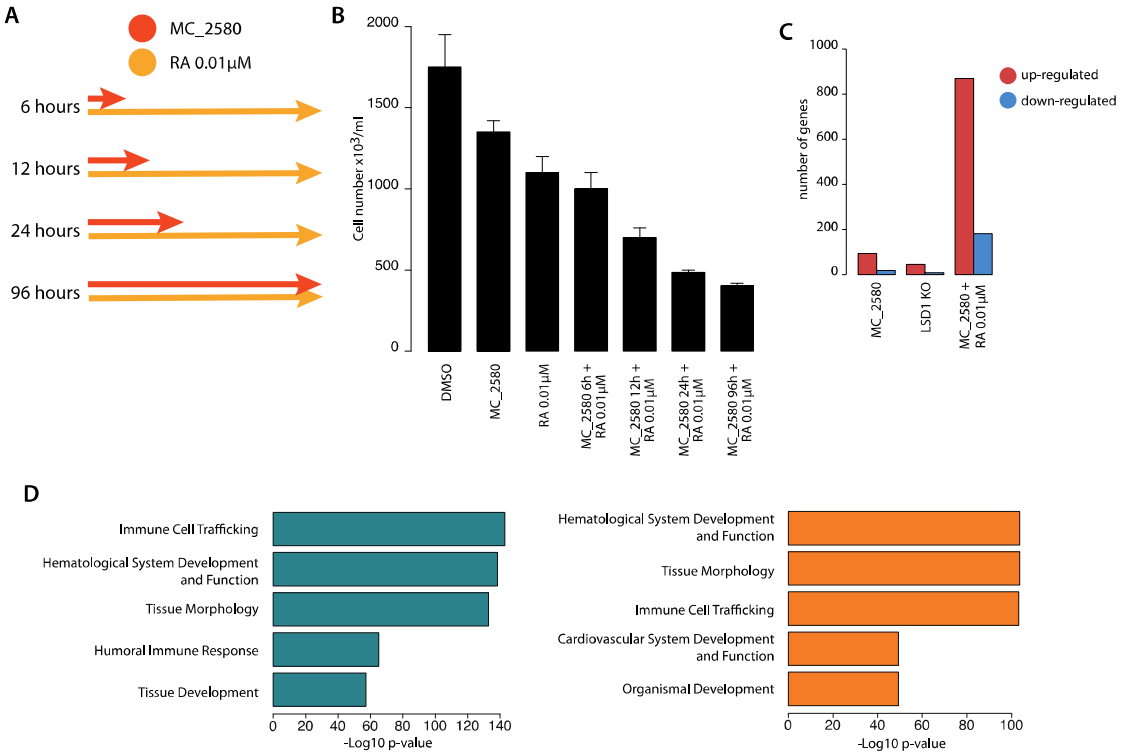

Figure S5. 24 hours of treatment with LSD1i are sufficient to sensitize NB4 cells to RA-induced differentiation.

A) Schematic representation of wash-out experiments. NB4 cells were co-treated with RA 0.01µM for 96h and MC_2580 2µM for 6, 12, 24 and 96 hours. At the indicated time-points, cells were washed several times, and medium containing only RA was added. **B)** NB4 cells were counted after 96 hours of treatment as in (A). 24 hours of LSD1 inhibition is sufficient to induce similar growth arrest to the longer treatment where the inhibitor is kept in the medium for 96 hours. **C)** RNA sequencing of NB4 KO cells. Barplot represents number of genes regulated (up or down regulated respect to the untreated control cells, RPKM>0.5, $\log_2$(FC)>1.5). MC_2580 and MC_2580 plus RA 0.01µM treated NB4 cells are reported also in figure 3a. **D)** Ingenuity Pathway Analysis (IPA) of genes up-regulated upon MC_2580 plus RA 0.01µM treatment (n = 868, left panel) or all genes up-regulated by RA 1µM treatment (n = 571, right panel). Adjusted p-value for each class is shown.

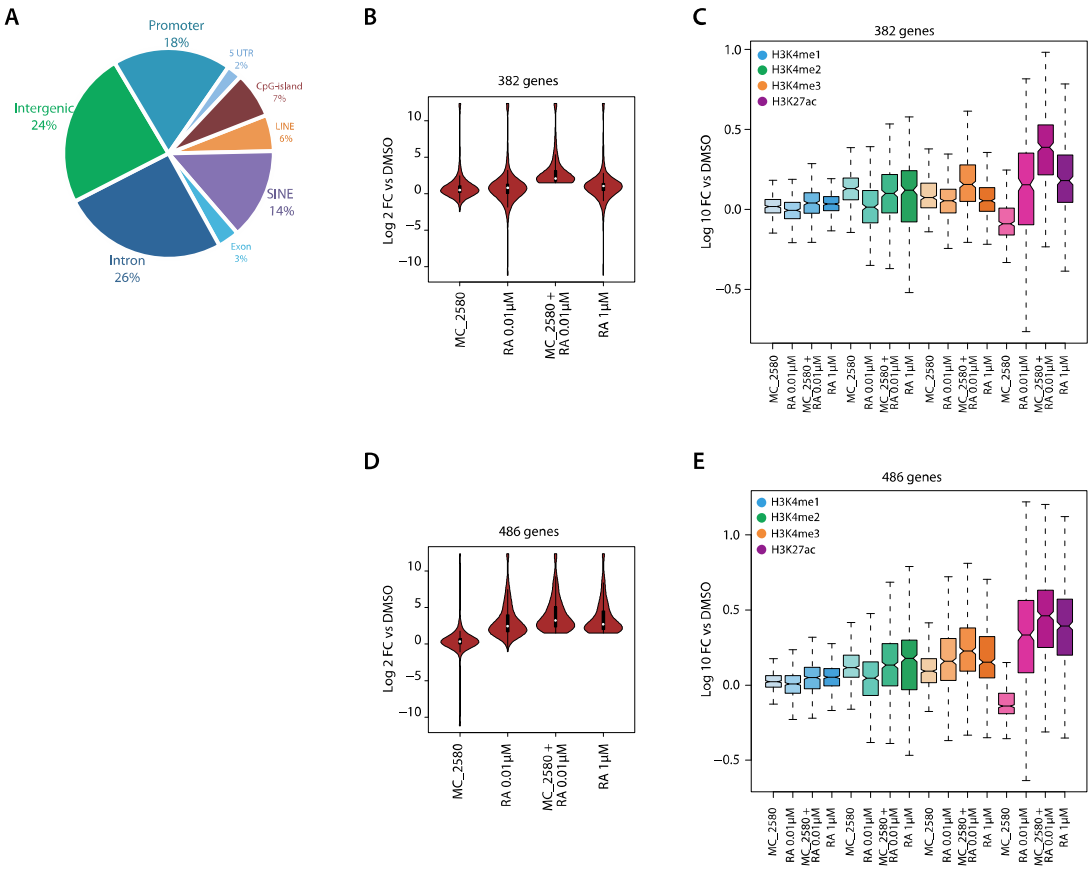

Figure S6. LSD1 inhibition and RA treatment remodel the chromatin landscape of NB4 cells.
A) Pie chart indicates genome annotations for 12698 LSD1 binding peaks. **B)** Violin plot representing the transcript levels (normalized RNA-seq intensities, $\log_2$ fold change) of NB4 cells treated as described for 24 hours. The plot refers to the same genes as in panel (C). **C)** Boxplot analysis of H3K4me, H3K4me2, H3K4me3 and H3K27ac enrichment upon indicated treatment at genes specifically up- regulated upon MC_2580 plus RA 0.01µM (n = 382, see figure 3b). Values are represented as fold change versus DMSO. **D)** Violin plot representing the transcript levels (normalized RNA-seq intensities, $\log_2$ fold change) of NB4 cells treated as described for 24 hours. The plots refer to genes up-regulated by MC_2580 plus RA 0.01µM, or by RA 1µM (n = 486). **E)** Boxplot analysis of H3K4me, H3K4me2, H3K4me3 and H3K27ac enrichment upon indicated treatment at the 486 genes shown in panel (D, see figure 3b). Values are represented as fold change versus DMSO.

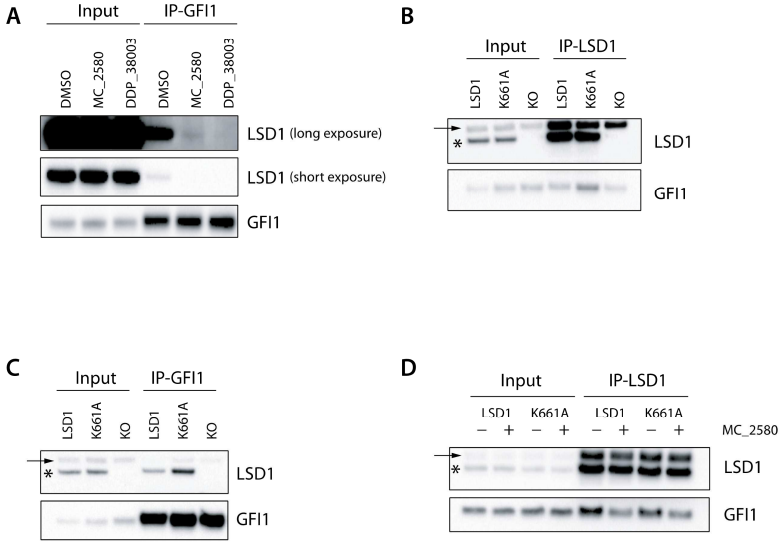

Figure S7. Pharmacological inhibition of LSD1 disrupts the interaction with GFI1.
A) Western blot analysis of LSD1 and GFI1 in GFI1 immunoprecipitations (IP) in NB4 cells treated for 24 hours with DMSO, MC_2580 2µM or DDP_38003 2µM. **B-C)** Western blot analysis of LSD1 and GFI1 in anti-LSD1 (IP-LSD1, panel B) or anti-GFI1 (IP-GFI1, panel C) immunoprecipitations in NB4 LSD1 KO cells transduced with Empty vector, wild-type or a catalytically inactive (K661A) LSD1 mutant. Asterisk marks LSD1, the arrow indicates a non-specific band. **D)** Western blot analysis of LSD1 and GFI1 in anti-LSD1 immunoprecipitations (IP-LSD1) in in NB4 LSD1 KO cells transduced with Empty vector, wild-type or a catalytically inactive (K661A) LSD1 mutant, and then treated with MC_2580 2µM (or DMSO alone, as control). Asterisk marks LSD1, the arrow indicates a non-specific band.

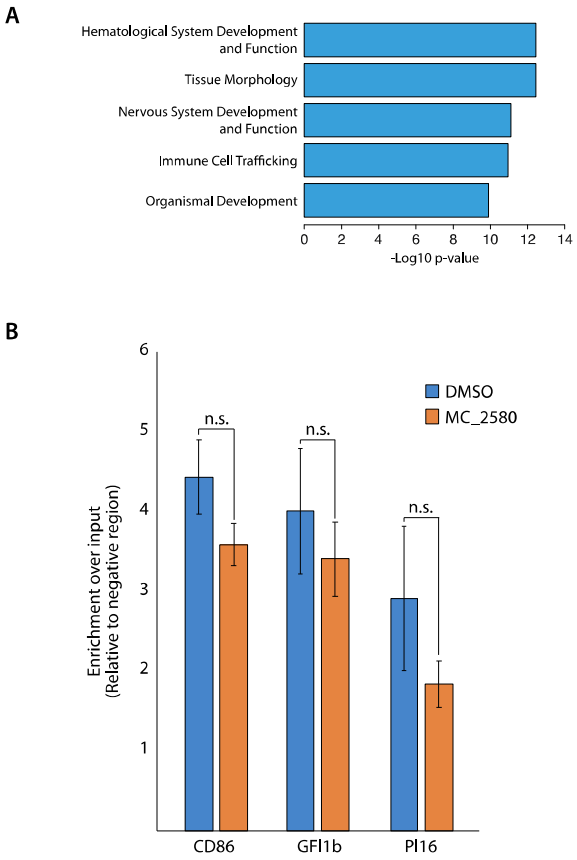

Figure S8. GFI1 recruits LSD1 to genes involved in hematopoietic cell differentiation and function.
A) Ingenuity Pathway Analysis (IPA) of genes associated to the 732 GFI1-bound regions that lose LSD1 ChIP-seq signal after treatment with MC_2580. **B)** GFI1 recruitment (ChIP-qPCR) before and after LSD1 inhibition at three regions showing overlapping binding of LSD1 and GFI1.

Table S1: The basal LSD1 interactome in NB4 cells.

Spreadsheet 1: Protein ratio distribution of the nuclear extract used as Input for the IP-LSD1 Forward 01 experiment (Rep1).

Spreadsheet 2: Analysis of LSD1 interactome from the IP-LSD1 Forward 01 experiment (Rep1), where competing soluble LSD1-peptide was added to the Light channel. Protein ratios were normalised on the median of the protein ratio distribution of the corresponding Input (spreadsheet 1), to correct for mixing errors. The protein ratio distributions of the IP obtained using a mixing model approach are displayed on the right. Putative LSD1 interactors of this replicate are shown in yellow.

Spreadsheet 3: Protein ratio distribution of the nuclear extract used as Input for the IP-LSD1 Forward 02 experiment (Rep2).

Spreadsheet 4: Analysis of LSD1 interactome from the IP-LSD1 Forward 02 experiment (Rep2), where competing soluble LSD1-peptide was added to the Light channel. Protein ratios were normalised on the median of the protein ratio distribution of the corresponding Input (spreadsheet 3). The protein ratio distributions of the IP obtained using a mixing model approach are displayed on the right. Putative LSD1 interactors of this replicate are shown in yellow.

Spreadsheet 5: Protein ratio distribution of the nuclear extract used as Input for the IP-LSD1 Reverse experiment (Rep3).

Spreadsheet 6: Analysis of LSD1 interactome from the IP-LSD1 Reverse experiment (Rep3), where competing soluble LSD1-peptide was added to the Heavy channel. Protein ratios were normalised on the median of the protein ratio distribution of the corresponding Input (spreadsheet 5). The protein ratio distributions of the IP obtained using a mixing model approach are displayed on the right. Putative LSD1 interactors of this replicate are shown in yellow.

Spreadsheet 7: List of the 147 common putative LSD1 interactors, extrapolated as top binders from the overlap of three SILAC-IP replicates. Proteins belonging to the CoREST complex are displayed in yellow.

Table S2: The dynamic LSD1 interactome upon treatment of NB4 cells with MC_2580.

Spreadsheet 1: Analysis of the changes in the LSD1 interactome upon drug treatment in the Forward experiment, where the drug was added to the Heavy channel. Proteins are ranked in an ascending H/L protein ratios, to highlight the interactors that are evicted upon drug treatment. Specific LSD1 interactors emerged from the basal interactome experiment are highlighted in yellow. Significantly evicted proteins are shown in pink while statistically recruited in green.

Spreadsheet 2: Analysis of the changes in the LSD1 interactome upon drug treatment in the Reverse experiment, where the drug was added to the Light channel. Proteins are ranked in an ascending L/H protein ratios, to highlight the interactors that are evicted upon drug treatment. Specific LSD1 interactors emerged from the basal interactome experiment are highlighted in yellow. Significantly evicted proteins are shown in pink while statistically recruited in green.

Spreadsheet 3: List of unchanged, evicted and recruited proteins in the LSD1 complexes upon drug treatment, in common between the two SILAC-IP replicates. Specific LSD1 interactors emerged from the basal interactome experiment are highlighted in yellow. Significantly evicted proteins are shown in pink while statistically recruited in green.

REFERENCES AND NOTES

1. Y. Shi, F. Lan, C. Matson, P. Mulligan, J. R. Whetstine, P. A. Cole, R. A. Casero, Y. Shi, Histone demethylation mediated by the nuclear amine oxidase homolog LSD1. *Cell* **119**, 941–953 (2004).

2. F. Forneris, C. Binda, M. A. Vanoni, A. Mattevi, E. Battaglioli, Histone demethylation catalysed by LSD1 is a flavin-dependent oxidative process. *FEBS Lett.* **579**, 2203–2207 (2005).

3. C. T. Foster, O. M. Dovey, L. Lezina, J. L. Luo, T. W. Gant, N. Barlev, A. Bradley, S. M. Cowley, Lysine-specific demethylase 1 regulates the embryonic transcriptome and CoREST stability. *Mol. Cell. Biol.* **30**, 4851–4863 (2010).

4. A. Sprüssel, J. H. Schulte, S. Weber, M. Necke, K. Händschke, T. Thor, K. W. Pajtler, A. Schramm, K. König, L. Diehl, P. Mestdagh, J. Vandesompele, F. Speleman, H. Jastrow, L. C. Heukamp, R. Schüle, U. Dührsen, R. Buettner, A. Eggert, J. R. Göthert, Lysine-specific demethylase 1 restricts hematopoietic progenitor proliferation and is essential for terminal differentiation. *Leukemia* **26**, 2039–2051 (2012).

5. M. A. Kerenyi, Z. Shao, Y.-J. Hsu, G. Guo, S. Luc, K. O'Brien, Y. Fujiwara, C. Peng, M. Nguyen, S. H. Orkin, Histone demethylase Lsd1 represses hematopoietic stem and progenitor cell signatures during blood cell maturation. *eLife* **2**, e00633 (2013).

6. S. Saleque, J. Kim, H. M. Rooke, S. H. Orkin, Epigenetic regulation of hematopoietic differentiation by Gfi-1 and Gfi-1b is mediated by the cofactors CoREST and LSD1. *Mol. Cell* **27**, 562–572 (2007).

7. L. T. van der Meer, J. H. Jansen, B. A. van der Reijden, Gfi1 and Gfi1b: Key regulators of hematopoiesis. *Leukemia* **24**, 1834–1843 (2010).

8. T. Möröy, L. Vassen, B. Wilkes, C. Khandanpour, From cytopenia to leukemia: The role of Gfi1 and Gfi1b in blood formation. *Blood* **126**, 2561–2569 (2015).

9. R. Thambyrajah, M. Mazan, R. Patel, V. Moignard, M. Stefanska, E. Marinopoulou, Y. Li, C. Lancrin, T. Clapes, T. Möröy, C. Robin, C. Miller, S. Cowley, B. Göttgens, V. Kouskoff, G. Lacaud,

GFI1 proteins orchestrate the emergence of haematopoietic stem cells through recruitment of LSD1. *Nat. Cell Biol.* **18**, 21–32 (2016).

10. K. Helin, S. Minucci, The role of chromatin-associated proteins in cancer. *Annu. Rev. Cancer Biol.* **1**, 355–377 (2017).

11. T. Schenk, W. C. Chen, S. Göllner, L. Howell, L. Jin, K. Hebestreit, H.-U. Klein, A. C. Popescu, A. Burnett, K. Mills, R. A. Casero Jr, L. Marton, P. Woster, M. D. Minden, M. Dugas, J. C. Y. Wang, J. E. Dick, C. Müller-Tidow, K. Petrie, A. Zelent, Inhibition of the LSD1 (KDM1A) demethylase reactivates the all-*trans*-retinoic acid differentiation pathway in acute myeloid leukemia. *Nat. Med.* **18**, 605–611 (2012).

12. W. J. Harris, X. Huang, J. T. Lynch, G. J. Spencer, J. R. Hitchin, Y. Li, F. Ciceri, J. G. Blaser, B. F. Greystoke, A. M. Jordan, C. J. Miller, D. J. Ogilvie, T. C.P. Somervaille, The histone demethylase KDM1A sustains the oncogenic potential of MLL-AF9 leukemia stem cells. *Cancer Cell* **21**, 473–487 (2012).

13. J. P. McGrath, K. E. Williamson, S. Balasubramanian, S. Odate, S. Arora, C. Hatton, T. M. Edwards, T. O'Brien, S. Magnuson, D. Stokoe, D. L. Daniels, B. M. Bryant, P. Trojer, Pharmacological inhibition of the histone lysine demethylase KDM1A suppresses the growth of multiple acute myeloid leukemia subtypes. *Cancer Res.* **76**, 1975–1988 (2016).

14. L. Altucci, S. Minucci, Epigenetic therapies in haematological malignancies: Searching for true targets. *Eur. J. Cancer* **45**, 1137–1145 (2009).

15. R. Nasr, M.-C. Guillemin, O. Ferhi, H. Soilihi, L. Peres, C. Berthier, P. Rousselot, M. Robledo-Sarmiento, V. Lallemand-Breitenbach, B. Gourmel, D. Vitoux, P. P. Pandolfi, C. Rochette-Egly, J. Zhu, H. de Thé, Eradication of acute promyelocytic leukemia-initiating cells through PML-RARA degradation. *Nat. Med.* **14**, 1333–1342 (2008).

16. J. Ablain, H. de The, Revisiting the differentiation paradigm in acute promyelocytic leukemia. *Blood* **117**, 5795–5802 (2011).

17. C. Binda, S. Valente, M. Romanenghi, S. Pilotto, R. Cirilli, A. Karytinos, G. Ciossani, O. A. Botrugno, F. Forneris, M. Tardugno, D. E. Edmondson, S. Minucci, A. Mattevi, A. Mai, Biochemical, structural, and biological evaluation of tranylcypromine derivatives as inhibitors of histone demethylases LSD1 and LSD2. *J. Am. Chem. Soc.* **132**, 6827–6833 (2010).

18. A.-T. Hauser, E.-M. Bissinger, E. Metzger, A. Repenning, U.-M. Bauer, A. Mai, R. Schüle, M. Jung, Screening assays for epigenetic targets using native histones as substrates. *J. Biomol. Screen.* **17**, 18–26 (2012).

19. S. Valente, V. Rodriguez, C. Mercurio, P. Vianello, B. Saponara, R. Cirilli, G. Ciossani, D. Labella, B. Marrocco, G. Ruoppolo, O. A. Botrugno, P. Dessanti, S. Minucci, A. Mattevi, M. Varasi, A. Mai, Pure diastereomers of a tranylcypromine-based LSD1 inhibitor: Enzyme selectivity and in-cell studies. *ACS Med. Chem. Lett.* **6**, 173–177 (2015).

20. P. Vianello, O. A. Botrugno, A. Cappa, R. D. Zuffo, P. Dessanti, A. Mai, B. Marrocco, A. Mattevi, G. Meroni, S. Minucci, G. Stazi, F. Thaler, P. Trifiró, S. Valente, M. Villa, M. Varasi, C. Mercurio, Discovery of a novel inhibitor of histone lysine-specific demethylase 1A (KDM1A/LSD1) as orally active antitumor agent. *J. Med. Chem.* **59**, 1501–1517 (2015).

21. J. Ablain, M. Leiva, L. Peres, J. Fonsart, E. Anthony, H. de Thé, Uncoupling RARA transcriptional activation and degradation clarifies the bases for APL response to therapies. *J. Exp. Med.* **210**, 647–653 (2013).

22. H. de Thé, Z. Chen, Acute promyelocytic leukaemia: Novel insights into the mechanisms of cure. *Nat. Rev. Cancer* **10**, 775–783 (2010).

23. J. H. A. Martens, A. B. Brinkman, F. Simmer, K.-J. Francoijs, A. Nebbioso, F. Ferrara, L. Altucci, H. G. Stunnenberg, PML-RARα/RXR alters the epigenetic landscape in acute promyelocytic leukemia. *Cancer Cell* **17**, 173–185 (2010).

24. Y. Lin, Y. Wu, J. Li, C. Dong, X. Ye, Y.-I. Chi, B. M. Evers, B. P. Zhou, The SNAG domain of Snail1 functions as a molecular hook for recruiting lysine-specific demethylase 1. *EMBO J.* **29**, 1803–1816 (2010).

25. H. P. Mohammad, K. N. Smitheman, C. D. Kamat, D. Soong, K. E. Federowicz, G. S. van Aller, J. L. Schneck, J. D. Carson, Y. Liu, M. Butticello, W. G. Bonnette, S. A. Gorman, Y. Degenhardt, Y. Bai, M. T. McCabe, M. B. Pappalardi, J. Kasparec, X. Tian, K. C. McNulty, M. Rouse, P. McDevitt, T. Ho, M. Crouthamel, T. K. Hart, N. O. Concha, C. F. McHugh, W. H. Miller, D. Dhanak, P. J. Tummino, C. L. Carpenter, N. W. Johnson, C. L. Hann, R. G. Kruger, A DNA hypomethylation signature predicts antitumor activity of LSD1 inhibitors in SCLC. *Cancer Cell* **28**, 57–69 (2015).

26. A. Adamo, B. Sesé, S. Boue, J. Castaño, I. Paramonov, M. J. Barrero, J. C. I. Belmonte, LSD1 regulates the balance between self-renewal and differentiation in human embryonic stem cells. *Nat. Cell Biol.* **13**, 652–659 (2011).

27. Y. Yu, K. Schleich, B. Yue, S. Ji, P. Lohneis, K. Kemper, M. R. Silvis, N. Qutob, E. van Rooijen, M. Werner-Klein, L. Li, D. Dhawan, S. Meierjohann, M. Reimann, A. Elkahloun, S. Treitschke, B. Dörken, C. Speck, F. A. Mallette, L. I. Zon, S. L. Holmen, D. S. Peeper, Y. Samuels, C. A. Schmitt, S. Lee, Targeting the senescence-overriding cooperative activity of structurally unrelated H3K9 demethylases in melanoma. *Cancer Cell* **33**, 322–336.e8 (2018).

28. A. Maiques-Diaz, G. J. Spencer, J. T. Lynch, F. Ciceri, E. L. Williams, F. M. R. Amaral, D. H. Wiseman, W. J. Harris, Y. Li, S. Sahoo, J. R. Hitchin, D. P. Mould, E. E. Fairweather, B. Waszkowycz, A. M. Jordan, D. L. Smith, T. C. P. Somervaille, Enhancer activation by pharmacologic displacement of LSD1 from GFI1 induces differentiation in acute myeloid leukemia. *Cell Rep.* **22**, 3641–3659 (2018).

29. J. Barth, K. Abou-El-Ardat, D. Dalic, N. Kurrle, A.-M. Maier, S. Mohr, J. Schütte, L. Vassen, G. Greve, J. Schulz-Fincke, M. Schmitt, M. Tosic, E. Metzger, G. Bug, C. Khandanpour, S. A. Wagner, M. Lübbert, M. Jung, H. Serve, R. Schüle, T. Berg, LSD1 inhibition by tranylcypromine derivatives interferes with GFI1-mediated repression of PU.1 target genes and induces differentiation in AML. *Leukemia* **33**, 1411–1426 (2019).

30. C. Lee, V. A. Rudneva, S. Erkek, M. Zapatka, L. Q. Chau, S. K. Tacheva-Grigorova, A. Garancher, J. M. Rusert, O. Aksoy, R. Lea, H. P. Mohammad, J. Wang, W. A. Weiss, H. L. Grimes, S. M. Pfister, P. A. Northcott, R. J. Wechsler-Reya, Lsd1 as a therapeutic target in Gfi1-activated medulloblastoma. *Nat. Commun.* **10**, 332 (2019).

31. R. Baron, C. Binda, M. Tortorici, J. A. McCammon, A. Mattevi, Molecular mimicry and ligand recognition in binding and catalysis by the histone demethylase LSD1-CoREST complex. *Structure* **19**, 212–220 (2011).

32. S.-E. Ong, B. Blagoev, I. Kratchmarova, D. B. Kristensen, H. Steen, A. Pandey, M. Mann, Stable isotope labeling by amino acids in cell culture, SILAC, as a simple and accurate approach to expression proteomics. *Mol. Cell. Proteomics* **1**, 376–386 (2002).

33. S. Minucci, S. Monestiroli, S. Giavara, S. Ronzoni, F. Marchesi, A. Insinga, D. Diverio, P. Gasparini, M. Capillo, E. Colombo, C. Matteucci, F. Contegno, F. Lo-Coco, E. Scanziani, A. Gobbi, P. G. Pelicci, PML-RAR induces promyelocytic leukemias with high efficiency following retroviral gene transfer into purified murine hematopoietic progenitors. *Blood* **100**, 2989–2995 (2002).

34. L. Di Croce, V. A. Raker, M. Corsaro, F. Fazi, M. Fanelli, M. Faretta, F. Fuks, F. L. Coco, T. Kouzarides, C. Nervi, S. Minucci, P. G. Pelicci, Methyltransferase recruitment and DNA hypermethylation of target promoters by an oncogenic transcription factor. *Science* **295**, 1079–1082 (2002).

35. A. R. Quinlan, I. M. Hall, BEDTools: A flexible suite of utilities for comparing genomic features. *Bioinformatics* **26**, 841–842 (2010).

36. D. Hnisz, B. J. Abraham, T. I. Lee, A. Lau, V. Saint-André, A. A. Sigova, H. A. Hoke, R. A. Young, Super-enhancers in the control of cell identity and disease. *Cell* **155**, 934–947 (2013).

37. M. Soldi, T. Bonaldi, The proteomic investigation of chromatin functional domains reveals novel synergisms among distinct heterochromatin components. *Mol. Cell. Proteomics* **12**, 764–780 (2013).

38. A. Shevchenko, H. Tomas, J. Havli, J. V. Olsen, M. Mann, In-gel digestion for mass spectrometric characterization of proteins and proteomes. *Nat. Protoc.* **1**, 2856–2860 (2006).

39. J. Rappsilber, M. Mann, Y. Ishihama, Protocol for micro-purification, enrichment, pre-fractionation and storage of peptides for proteomics using StageTips. *Nat. Protoc.* **2**, 1896–1906 (2007).

40. I. Barozzi, A. Termanini, S. Minucci, G. Natoli, Fish the ChIPs: A pipeline for automated genomic annotation of ChIP-Seq data. *Biol. Direct* **6**, 51 (2011).

41. B. Langmead, C. Trapnell, M. Pop, S. L. Salzberg, Ultrafast and memory-efficient alignment of short DNA sequences to the human genome. *Genome Biol.* **10**, R25 (2009).

42. M. Cesaroni, D. Cittaro, A. Brozzi, P. G. Pelicci, L. Luzi, CARPET: A web-based package for the analysis of ChIP-chip and expression tiling data. *Bioinformatics* **24**, 2918–2920 (2008).

43. F. Ramírez, D. P. Ryan, B. Grüning, V. Bhardwaj, F. Kilpert, A. S. Richter, S. Heyne, F. Dündar, T. Manke, deepTools2: A next generation web server for deep-sequencing data analysis. *Nucleic Acids Res.* **44**, W160–W165 (2016).

44. C. Trapnell, B. A. Williams, G. Pertea, A. Mortazavi, G. Kwan, M. J. van Baren, S. L. Salzberg, B. J. Wold, L. Pachter, Transcript assembly and quantification by RNA-Seq reveals unannotated transcripts and isoform switching during cell differentiation. *Nat. Biotechnol.* **28**, 511–515 (2010).

45. J. Cox, M. Mann, MaxQuant enables high peptide identification rates, individualized p.p.b.-range mass accuracies and proteome-wide protein quantification. *Nat. Biotechnol.* **26**, 1367–1372 (2008).

46. J. Cox, N. Neuhauser, A. Michalski, R. A. Scheltema, J. V. Olsen, M. Mann, Andromeda: A peptide search engine integrated into the MaxQuant environment. *J. Proteome Res.* **10**, 1794–1805 (2011).

47. T. M. Maile, A. Izrael-Tomasevic, T. Cheung, G. D. Guler, C. Tindell, A. Masselot, J. Liang, F. Zhao, P. Trojer, M. Classon, D. Arnott, Mass spectrometric quantification of histone post-translational modifications by a hybrid chemical labeling method. *Mol. Cell. Proteomics* **14**, 1148–1158 (2015).